fluids

MDPI

Article

Experimental Research on Ship Wave-Induced Motions of Tidal Turbine Catamaran

Tinghui Liu, Xiwu Gong *, Zijian Yu and Yonghe Xie

College of Ship and Maritime, Zhejiang Ocean University, Zhoushan 316022, China; 13728441141@163.com (T.L.); 13868244330@163.com (Z.Y.); xieyh@zjou.edu.cn (Y.X.)
* Correspondence: gxw@zjou.edu.cn

Abstract

In this research, the effect of ship navigation on the mooring system of a deep-sea floating tidal energy platform is experimentally investigated. Hydrodynamic experiments were conducted on a figure-of-eight mooring system with a KCS ship (KRISO Container Ship) as the sailing ship model and a catamaran as the carrier model of the tidal current energy generator under the combined effect of waves and ocean currents. The experimental results show that the increase in ship speed increases the amplitude of the carrier motion re-response. When the ship speed increases from 1.2 m/s to 1.478 m/s, the roll amplitude increases by 220%. At the same time, a decrease in the distance and draft of the navigating vessel also increases the amplitude of the motion response. Then, the actual sea conditions are simulated by the combined effect of ship waves and regular waves. As the wave period decreases and the height increases, the platform motion response is gradually reduced by the ship-generated waves. These findings provide important insights for optimizing the mooring system design in wave-dominated marine environments.

Keywords: mooring system; motion response; numerical simulation calculation; experiment; catamaran

check for updates

Academic Editors: D. Andrew S. Rees and Giuliano De Stefano

Received: 16 May 2025
Revised: 9 July 2025
Accepted: 30 July 2025
Published: 4 August 2025

Citation: Liu, T.; Gong, X.; Yu, Z.; Xie, Y. Experimental Research on Ship Wave-Induced Motions of Tidal Turbine Catamaran. *Fluids* **2025**, *10*, 205. https://doi.org/10.3390/fluids10080205

Copyright: © 2025 by the authors. Licensee MDPI, Basel, Switzerland. This article is an open access article distributed under the terms and conditions of the Creative Commons Attribution (CC BY) license (https://creativecommons.org/licenses/by/4.0/).

1. Introduction

Against the backdrop of the accelerating global energy transition, the limitations of traditional fossil energy are becoming increasingly prominent. The International Energy Agency (IEA) predicts that, by 2040, renewable energy will need to meet 65% of the global energy increment demand. In the diversified renewable energy system, ocean energy has become a strategic focus, with its theoretical reserves of 3.8×10^4 TWh/year (equivalent to twice the current global electricity consumption) [1]. Tidal current energy has been listed by the European Union as a core direction of the 2050 Marine Energy strategy due to its unique physical properties [2]. The trend can take into account energy intensity, stability, and predictability. O. Roberts [3], studying energy density, reported that the tidal current energy density at a flow velocity of 3 m/s reaches 14.5 kW/m^2, which is four times that of wind energy at the same wind speed. Data from the International Renewable Energy Agency (IRENA) shows that the global installed capacity of tidal current energy exceeded 200 MW in 2023. Dai [4] evaluated the potential for developing tidal flow energy in the Zhoushan area of China using a numerical model. By comparing the maximum average tidal flow power density of different channels, it was shown that the tidal current energy in this area has high development potential and economic feasibility. Spicer [5] focused on the Aleutian Islands region of Alaska, conducting an in-depth analysis of how mixed tidal

regimes influence the spatial distribution of tidal current energy potential and revealing its seasonally modulated variability patterns.

The motion response problem has always been the focus of research on oceanic floats and has been studied by many scholars in conjunction with waves and currents. Sun [6] introduced a Laplace domain-based method for estimating wave heights from the transient motion response of a floating body. The method provides an effective way to invert the wave characteristics from the float motion data by establishing a mathematical relationship between the motion response of the float and the wave excitation. Zang [7] conducted an in-depth investigation of the motion response characteristics of a floating wind turbine with a semi-submersible foundation by experimental means, aiming to obtain a comprehensive understanding of its dynamical behavior under different sea states. In recent years, significant progress has been made in the research of carriers for tidal current power generation devices. Wang [8] designed a submersible carrier for tidal generators and used computational fluid dynamics methods to study the smooth flow distribution of the turbine during operation. It was determined that this design improved the energy acquisition and efficiency of the turbine for tidal energy. Sheng [9] analyzed the hydrodynamic loads of the double-blade fixed-pitch vertical-axis turbine of the Haineng I 2×150 kW floating tidal power station in the same direction of waves and water flow and verified that, under the same wave height conditions, the ultimate load of the main shaft increases with the increase in wave height.

The economic development of shipping has led to increasingly frequent maritime traffic, and the ship waves caused by ship navigation can impact not only other ships but also fixed and floating platforms at sea. Some studies on fixed and floating carriers have considered the effects of ship waves and incorporated them into their research. Huang [10] employed a three-dimensional numerical simulation approach based on the resolution of the Navier–Stokes equations to ascertain the causal link between ship waves and the erosion phenomenon of river channel banks, as well as to offer critical conditions for the protection of these banks. By examining the decrease in wave elevation near the banks of the waterway, it was demonstrated that the normal impact forces and tangential shear stresses caused by ship waves are the primary culprits in the erodibility of riverbanks. Zhang [11], taking the MASHCON2022 benchmark model test cases as the research subject, employed the Unsteady Reynolds-Averaged Navier–Stokes (URANS) method coupled with dynamic overlapping grid technology to simulate the entire process of a ship passing by a moored vessel. By simulating four acceleration patterns of the navigating ship, the research validated the impact of the navigating ship on the moored ship during the initial acceleration phase. Wu [12] focused on dynamic response and vibration control problems of deep-water bridge piers under ship wave excitation. By deeply analyzing the action mechanism of ship waves on deep-water bridge piers, we aim to reveal their dynamic response characteristics and explore effective vibration control strategies to ensure the safety and stability of deep-water bridge structures.

At present, academics mostly focus on the structural research of tidal buoy carriers under the action of regular waves [13,14], while there is a relative lack of investigative research on their stability under the influence of ship traveling waves. In fact, ship waves generated by different ship speeds, ship spacing parameters, and draught conditions during ship navigation can significantly perturb the stability of the carrier, which, in turn, reduces the power generation efficiency of the tidal energy generator. The research will be presented across five sections: 1. Section 1 is responsible for introducing the established research results on ship traveling waves and carrier motion; 2. Section 2 is responsible for demonstrating the theoretical framework applied in the research; 3. Section 3 provides a finely detailed introduction of the experimental equipment and model; 4. Section 4 is

responsible for the visual presentation and in-depth analysis of the experimental data; and, finally, 5. Section 5 presents the conclusions drawn from the thesis and points out the shortcomings of the research. In this research, a catamaran configuration was innovatively introduced into the field of floating tidal energy carriers, and the 3600 TEU KCS container ship designed by KRISO Research Institute of Korea was used as the sailing vessel to form a multi-body coupled experimental whole. Through the combination of theoretical modeling and tank experiments, the motion response law of the six-degree-of-freedom catamaran was systematically analyzed under variable environmental parameters, providing a novel technical idea and experimental basis for the cross-field integration of ship and tidal energy development and utilization and expanding the design boundaries and application scenarios of floating tidal energy carriers.

2. Methods

2.1. Ship Wave Theory

As shown in Figure 1, the main characteristics of ship waves are as follows: The size of the Kelvin angle is independent of the ship's speed, and it is invariant to the ship's speed. The ship speed primarily modulates wave amplitude while preserving the Kelvin angle. When the ship speed is low, the divergent wave is the main wave system. With the increase in the ship speed, the transverse wave gradually strengthens, while the stray wave gradually weakens. The magnitude and direction of the scattered waves are related to the ship type, speed, etc. The scattered waves at the bow and stern of the ship, as well as the scattered waves and transverse waves, do not interfere with each other [15].

$$T = \sqrt{\frac{2\pi\lambda}{g}} \tag{1}$$

$$c = \frac{\lambda}{T} = \sqrt{\frac{g\lambda}{2\pi}} \tag{2}$$

$$\omega = \frac{2\pi}{T} = \sqrt{\frac{2\pi g}{\lambda}} = \sqrt{kg} \tag{3}$$

$$\lambda_1 = \frac{2\pi v^2}{g} \tag{4}$$

$$\lambda_2 = \frac{2\pi v^2}{g} cos^2\Phi \tag{5}$$

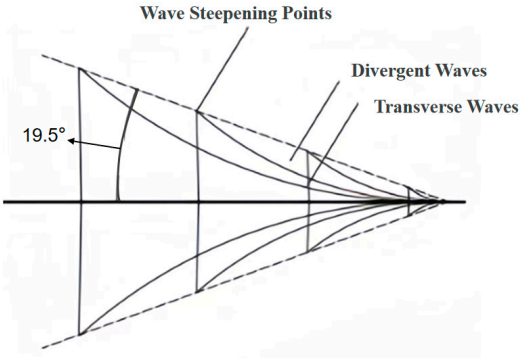

Figure 1. Diagram of ship wave.

In the above formula, k is the wave number, g is the acceleration due to gravity, Φ is the Kelvin angle, λ_1 is the wavelength of the transverse wave, λ_2 is the wavelength of the scattered wave, and v is the velocity of the ship.

The advancing speed of the transverse wave of the traveling wave of a ship is the same as the moving speed of the origin of the disturbed pressure. With the gradual deepening of the research on the Kelvin pressure disturbance theory by scholars from various countries, the theoretical research on the traveling wave of a ship is also constantly improving. The change in the wave height of the traveling wave of a ship is mainly affected by the shape and speed of the ship.

The phase velocity of transverse waves in a ship's wake matches the propagation speed of the pressure disturbance source. As research on Kelvin wake theory has progressed, the understanding of ship waves has significantly advanced. The amplitude of ship waves is primarily determined by hull geometry and vessel speed.

Considering the relationship between the ship wave and the type and speed of the ship, the formula for calculating the ship wave is

$$H = k \cdot \frac{v^2}{g} \cdot \left(\frac{B}{L}\right)^{\frac{1}{2}} \tag{6}$$

In the formula, k is the correction coefficient, which is generally taken as 0.2–0.5. In this research, the correction coefficient for the selected KCS ship is $k = 0.2$. B is the width of the ship; L is the captain. v is the sailing speed of the ship; g is the acceleration due to gravity [16].

2.2. Motion Response Motion Equation

The expression of the motion equation of a floating body under the combined action of wind, waves, and currents is as follows [17]:

$$M(\omega)\ddot{x} + \lambda(\omega)\ddot{x} + C(\omega)\dot{x} + K(\omega)x = F_{\text{wind}} + F_{\text{current}} + F_{\text{wave}} + F_{\text{mooring}} \tag{7}$$

In the formula, M represents the mass matrix of the floating body; C represents the damping matrix of the floating body; K represents the stiffness matrix of the floating body; F_{wind} represents the wind load; F_{curret} represents the flow load; F_{wave} represents the wave load; and F_{mooring} represents the mooring force provided by the mooring system.

The added mass matrix is determined in this research using thin-body approximation within potential flow theory, accounting for the hydrodynamic characteristics of the catamaran configuration. Following Faltinsen's theoretical framework, the added mass coefficients demonstrate distinct dependencies on (1) hull separation distance for transverse motions and (2) demi-hull cross-sectional geometry for longitudinal motions. The slender-body formulation yields the following expressions for added mass estimation:

$$m_{a,x} = \rho L B C_{a,x} \tag{8}$$

$$m_{a,y} = \rho L B C_{a,y} \tag{9}$$

$$I_{a,roll} = \rho L B (B/2)^2 C_{a,roll} \tag{10}$$

where ρ is the water density; L is the length of the hull; B is the spacing between the centers of the two hulls; and $C_{a,x}$, $C_{a,y}$, and $C_{a,roll}$ are the coefficients of the added mass in the surge, sway, and roll directions, respectively. These coefficients are determined according to the geometrical parameters and kinematic state of the catamaran, with reference to relevant literature and experimental data.

For the damping matrix, the effects of viscous damping and rising wave damping are considered together. The viscous damping is obtained by calculating the frictional resistance on the hull surface, while the rising wave damping is estimated based on the

wave generation characteristics of the catamaran in different motion states. The following empirical equations were used to calculate the damping coefficients for each degree of freedom:

$$c_x = \rho LBC_{d,x} \tag{11}$$

$$c_y = \rho LBC_{d,y} \tag{12}$$

$$c_{pitch} = \rho LBC_{d,pitch} \tag{13}$$

where $C_{d,x}$, $C_{d,y}$, and $C_{d,pitch}$ are the damping coefficients in the surge, sway, and longitudinal rocking directions, respectively.

The restoring force matrix is derived from the hydrostatic properties of the catamaran, incorporating both buoyancy and stability considerations. The diagonal elements characterize the direct restoring forces and moments, governed by the equilibrium between buoyancy and gravitational forces. The off-diagonal elements account for coupling effects between different motion degrees of freedom, reflecting the interconnected nature of the catamaran's hydrostatic response. The matrix formulation is expressed as

$$k_x = \rho gV \tag{14}$$

$$k_{roll} = \rho gVGM \tag{15}$$

where V is the volume of discharged water, and GM is the initial stability height.

2.3. The Principle of the Push-Type Regular Wave Generator

The form of wave generation used for regular wave generation in this research is mainly push wave generation; the offshore wave tanks of the Danish Hydraulic Institute (DHI) and the Norwegian Marintek wave tank use this form. Its working principle is described below [18].

① Control system parameter input: Set the target wave parameters—wave height H, period T, and water depth h—and calculate the push plate movement parameters (amplitude S, frequency $f = 1/T$).

② Generate push plate movement: The servo motor/hydraulic cylinder drives the pusher plate to perform simple harmonic motion; the specific formula is

$$x(t) = S \cdot sin(2\pi ft) \tag{16}$$

where $x(t)$ represents the instantaneous displacement of the pusher plate.

③ Wave formation: The push plate pushes the water body to generate traveling waves, and the waveform satisfies the linear wave theory:

$$\eta(x,t) = 2Hcos(kx - \omega t) \tag{17}$$

where $\eta(x,t)$ represents the wave surface elevation, k represents the wave number $k = 2\pi/\lambda$, and ω represents the angular frequency $\omega = 2\pi/T$.

④ Wave dissipation treatment: A porous wave-absorbing beach is installed at the downstream end to suppress reflected waves, achieving a reflection coefficient of less than 5% ($R < 0.05$).

3. Experimental Arrangement

3.1. Overview of the Experimental Tank and Experimental Model

This experiment was conducted in the experimental tank of Zhejiang Ocean University. The experimental tank is shown in Figure 2. The size parameters of the tank are as follows:

the length of the tank is 120 m, the width of the tank is 6 m, and the depth of the tank is 3.5 m. At the same time, the experimental tank is equipped with a wave generator with a wave generation period of 0.5–5 s, simulating regular waves.



Figure 2. Experimental tank laboratory of Zhejiang Ocean University.

The experimental study employed the KRISO Container Ship (KCS) model [19], a standardized container ship hull form developed by the Korea Research Institute of Ships and Ocean Engineering (KRISO) for hydrodynamic research and computational fluid dynamics (CFD) validation. The principal dimensions and experimental setup are detailed in Figure 3 and Table 1. The weight scaling of the sailing vessel is not considered in this research, mainly due to the fact that the central focus of this research is on the mechanism of the influence of the ship's traveling wave on the action of the floating body. In the experimental design, in order to generate the ship's traveling wave, a bracket is fixed on the hull, and the bracket parameters are precisely adjusted to change the draft depth of the hull. The change in the draft depth of the hull will lead to a change in the interaction between the hull and the water surface, which will stimulate the traveling waves with different characteristic parameters. This adjustment method can effectively simulate a variety of traveling wave patterns, which meets the needs of the research of the impact of the traveling wave on the floating body and provides a strong support for the in-depth investigation of the mechanism of its action.



(**a**) (**b**)

Figure 3. Model of the ship. (**a**) Ship model in 3D software Simcenter STAR-CCM+ 2210 (17.06.007-R8). (**b**) Ship model for experiment.

Table 1. Main parameters of the ship (scale ratio λ = 1:67).

Parameter	Actual Dimensions	Model Dimensions
Ship's length/m	230.00	3.42
Ship's width/m	32.30	0.48
Depth/m	10.90	0.16
Draft volume/m^3	52,030.00	0.17

As shown in Figure 4, the floating tidal energy converter adopted in this experiment utilizes a catamaran configuration [20]. A prototype catamaran with 50 m length was selected as the reference geometry, and its precisely scaled down model was developed through 3D parametric modeling. This numerical model was then physically fabricated according to the same scale ratio (λ) used for the navigation vessel model. The complete dimensional specifications for both prototype and experimental models are systematically compared in Table 2, including all principal particulars and hydrodynamic-relevant features.

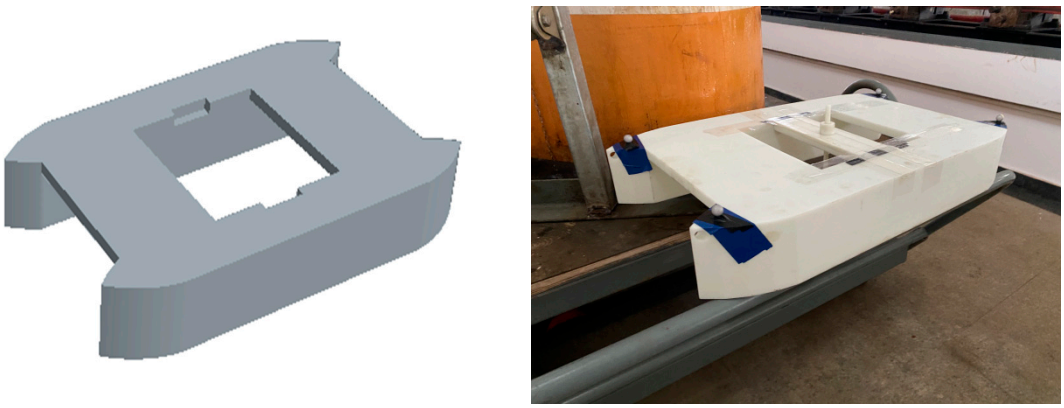

(**a**) (**b**)

Figure 4. Comparison of hydraulic turbine platform model. (**a**) Model picture. (**b**) Physical picture.

Table 2. Main parameters of the catamaran (scale ratio λ = 1:67).

Parameter	Actual Dimensions	Model Dimensions
Ship 's length/m	51.45	0.77
Ship 's width/m	30.94	0.46
Ship's height/m	7.73	0.12
Depth/m	3.00	0.04
Distance between bodies/m	20.18	0.30

To control the positioning stability of the catamaran floating body under the action of waves, the experiment adopted four steel cables with a diameter of 2 mm and a length of 5 m to form a symmetrical radial mooring layout [21]. The ends of the cables were connected to the bottom of the tank by connecting heavy objects. This configuration can effectively limit the carrier drift while avoiding the introduction of additional motion constraint torques. It should be noted that this experiment focuses on the analysis and research of the motion response of catamarans, and the mooring system only exists as the physical anchor point of the motion reference frame. Therefore, analysis of structural responses, such as changes in the mechanical properties and the dynamic tension of mooring materials, is not within the scope of this text.

As shown in Figure 5, in this experimental research, the six-degree-of-freedom (6DOF) motions of the moored floating structure were captured using an MC4000 high-speed

camera system from Qingtong Vision (Nantong, China). The camera's specifications are detailed in Table 3. Prior to data acquisition, a three-stage calibration procedure was performed: (1) dynamic tracking of reflective markers, (2) establishment of the global coordinate system, and (3) construction of a real-time Kalman filter-based rigid body model.

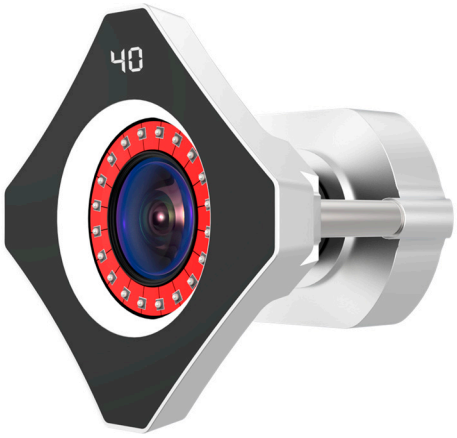

Figure 5. Motion capture camera.

Table 3. Main parameters of the motion capture camera.

Parameters	
Resolution	2048 × 2048
Maximum Frame Rate	180 fps
Focal Length	12 mm
Horizontal Field of View/Vertical Field of View	53°/53°
Furthest Passive Tracking Distance	30 m
Furthest Active Tracking Distance	60 m
3D Accuracy	+/−0.06 mm
Interface Type	RJ45
Number of LEDs	20
Total Power	6–18 w

The devices used in this experiment to haul the sailing vessel to move were a winch motor and a rigid rope. The winches used in this experiment are shown in Figure 6, and their parameters are shown in Table 4.

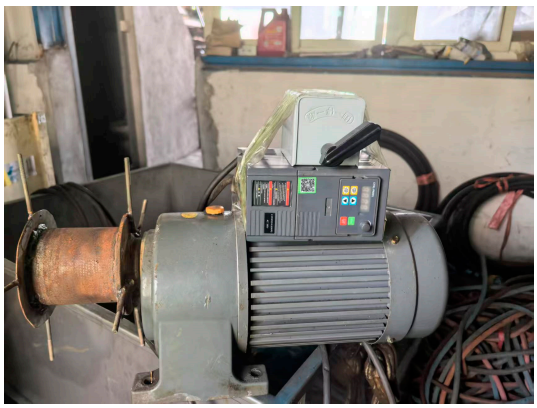

Figure 6. Winch motor.

Table 4. Main parameters of the winch motor.

Parameters	
Power	2.2 kW
Rated speed	1450 rpm
Rated frequency	50 Hz
Reel diameter	100 mm
Reducer speed ratio	1:5

3.2. Experimental Arrangement and Experimental Procedures

In the experiment, an advanced optical motion capture system was adopted to accurately measure the motion response of the floating carrier. The experimental layout is shown in Figure 7. The experimental system replaces the traditional trailer with the winch—equipped with a tow rope mechanism—and combines the sliding rail type ship fixing device to achieve the stable linear motion of the ship, effectively eliminating the interference of mechanical vibration and the problem of hull yaw. The motion capture system consists of three high-speed infrared cameras forming a triangulation array. Five reflective marking points are arranged at the key positions of the carrier to establish a rigid body model, achieving precise collection of six-degree-of-freedom motion. Actual pictures from some experiments are shown in Figure 8.

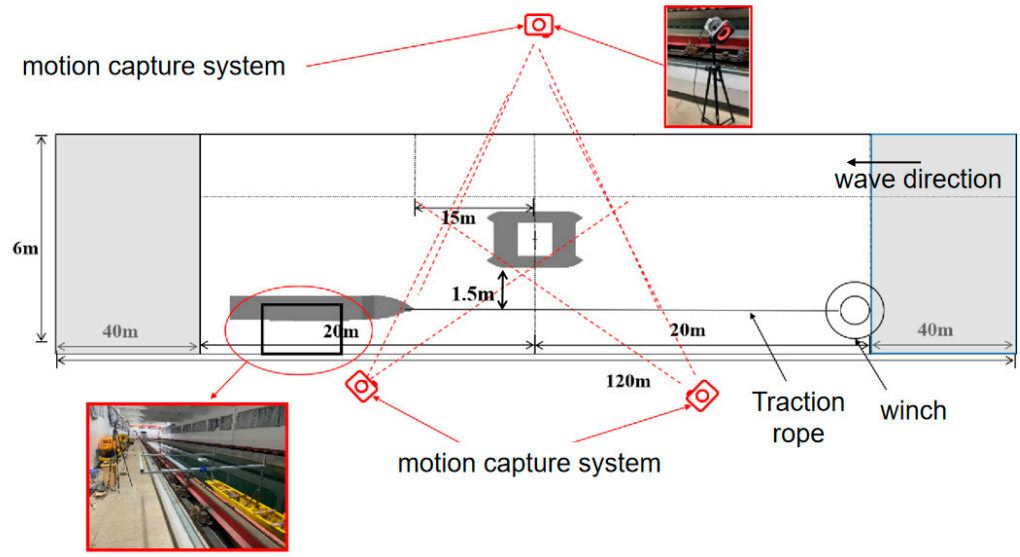

Figure 7. Experimental layout.



(**a**) (**b**)

Figure 8. Experimental case in the experimental tank. (**a**) Ship wave identity. (**b**) The ship wave affects the carrier.

In the experimental process, the real-time feedback position data are collected and compared and processed with the initial position data, so as to obtain the real-time change data. Spatial displacements were recorded as Cartesian coordinates (X, Y, Z), while attitude data were stored as normalized quaternions q = (r, x, y, z). To obtain more intuitive parameters of the ship's motion attitude, it is necessary to convert quaternions into Euler angles for representation. The specific conversion formulas for pitch, roll, and yaw are as follows:

$$Pitch = \arcsin(-2(xz - yr)) \tag{18}$$

$$Roll = arctan2\Big(2(yz + xr), r^2 + x^2 - y^2 - z^2\Big) \tag{19}$$

$$Yaw = arctan2\Big(2(xy + zr), r^2 - x^2 - y^2 + z^2\Big) \tag{20}$$

In experimental research, the design of experimental steps is crucial because it is directly related to the accuracy and reliability of experimental data. The rationality and scientific details of the experimental steps will largely affect the correctness of the experimental results. The steps of this experiment are shown in Figure 9. The specific experimental steps are as follows: (1) Install the sailing ship model in the experimental tank, and at the same time, arrange the winch motor, ship fixing bracket, and hauling rope. (2) Position the catamaran carrier model and connect the carrier and the weight at the bottom of the tank with the mooring cable. (3) According to the position of the catamaran carrier model, adjust the position of the three cameras of the dynamic trapping system to ensure that the motion of the carrier is clearly captured. (4) Start the winch motor and the wavemaker, and then verify the wave height, period, and ship traveling wave trajectory of the rule wave. If it is not reasonable, adjust it; otherwise, start the experiment. Obtain the six-degree-of-freedom change data of the catamaran carrier by changing the speed of the ship, the distance between the ship and the carrier, and the draught of the sailing ship. (5) Integrate the data and convert them to draw the time-domain change charts, before obtaining the curve change charts and conclusions.

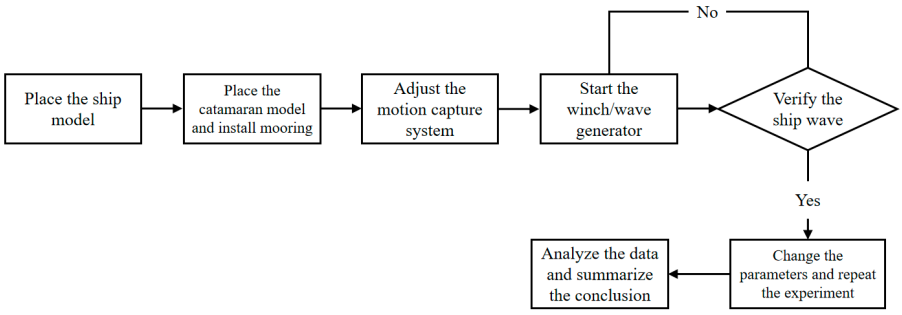

Figure 9. Flowchart of the experiment.

This research is based on the MC4000 motion capture system (sampling rate 200 Hz, nominal accuracy ±0.1°), tested under strictly controlled environmental conditions. The uncertainty mainly originates from 1. wave repeatability error (CV = 4.5%), which is statistically calculated through multiple repetitive tests, and 2. environmental disturbance contributions: temperature drift, humidity refractive index change, and light fluctuation. In order to reduce the impact of these conditions on the experimental results, in this study, we aimed to conduct experiments in the same luminance scenario, as well as under the same temperature and humidity conditions, and verify that the external condition error is within the acceptable range through repeated experiments.

4. Results and Analysis

This experiment was designed to focus on key parameters such as regular waves, ship distance, ship speed, the regular wave period, and draft of the navigating vessel, and conduct systematic control experiments. The experiment also focused on analyzing and comparing data under the following three working conditions: the action of regular waves alone, the action of traveling waves alone, and the superimposed action of traveling waves and regular waves. Through in-depth analysis of the experimental data of different working conditions and parameter combinations, this research will systematically explore the influence laws of various factors on the motion response of the floating carriers of mooring catamarans and ultimately draw corresponding conclusions.

In this experiment, we adopted an infrared motion capture system to monitor the motion response of the floating body in real time. This system has high measurement accuracy and anti-interference ability and is not affected by external electromagnetic noise. However, under different environmental conditions, changes in temperature, humidity, and light intensity may cause a certain degree of interference to the transmission and reception of infrared signals, thereby introducing certain measurement errors. To effectively reduce the impact of such errors on the experimental results and ensure the reliability and accuracy of the data, we conducted at least three repeated measurements for each group of experiments. Through the statistical analysis of the repeated experimental data, it was found that the experimental error was controlled within an acceptable range, and the data had good consistency and repeatability. Therefore, this paper selects one group of representative experimental results for detailed analysis and discussion to verify the errors of the experiments and ensure the scientificity and rigor of the research conclusions at the same time.

As shown in Figure 10, two experiments of six-degree-of-freedom kinematic response curves are demonstrated for a ship speed of 1.478 m/s and a ship spacing of 1.5 m. The response curves of the six-degree-of-freedom kinematic response are shown in Figure 10. Neglecting the problem of acquisition start time, the two experiments have the same experimental data pattern, and at the same time, by calculating the peak value of each motion response, the error of the peak value of each motion response is less than 5%, so the experimental setup produces less error and meets the rigor requirements of experimental papers.

By comparing and analyzing the maximum values of the variation amplitude of the six degrees of freedom of the two groups of data, As shown in Table 5, the results show that the errors were controlled to be around 10%. Specific quantitative assessments showed that the difference in means was less than 5 per cent, the standard deviation was maintained at a low level, the root mean square error (RMSE) was less than 0.15, and the overlap of the 95 per cent confidence intervals was high. All these indicators confirm the reliability and reproducibility of the experimental results. The trends of the two groups of data are highly consistent, and the corresponding error values are within acceptable limits, which indicates that the experimental results have good reliability and reproducibility.

Table 5. Peak data comparison and corresponding error values.

	First Test	Second Test	Error
Pitch	4.4746	4.19355	6.3%
Roll	−3.10379	−2.7708	10.7%
Yaw	2.61638	2.60282	0.5%
Sway	−81.74	−78.1	4.5%
Heave	−13.943	−12.145	12.9%
Surge	−72.306	−66.597	7.9%

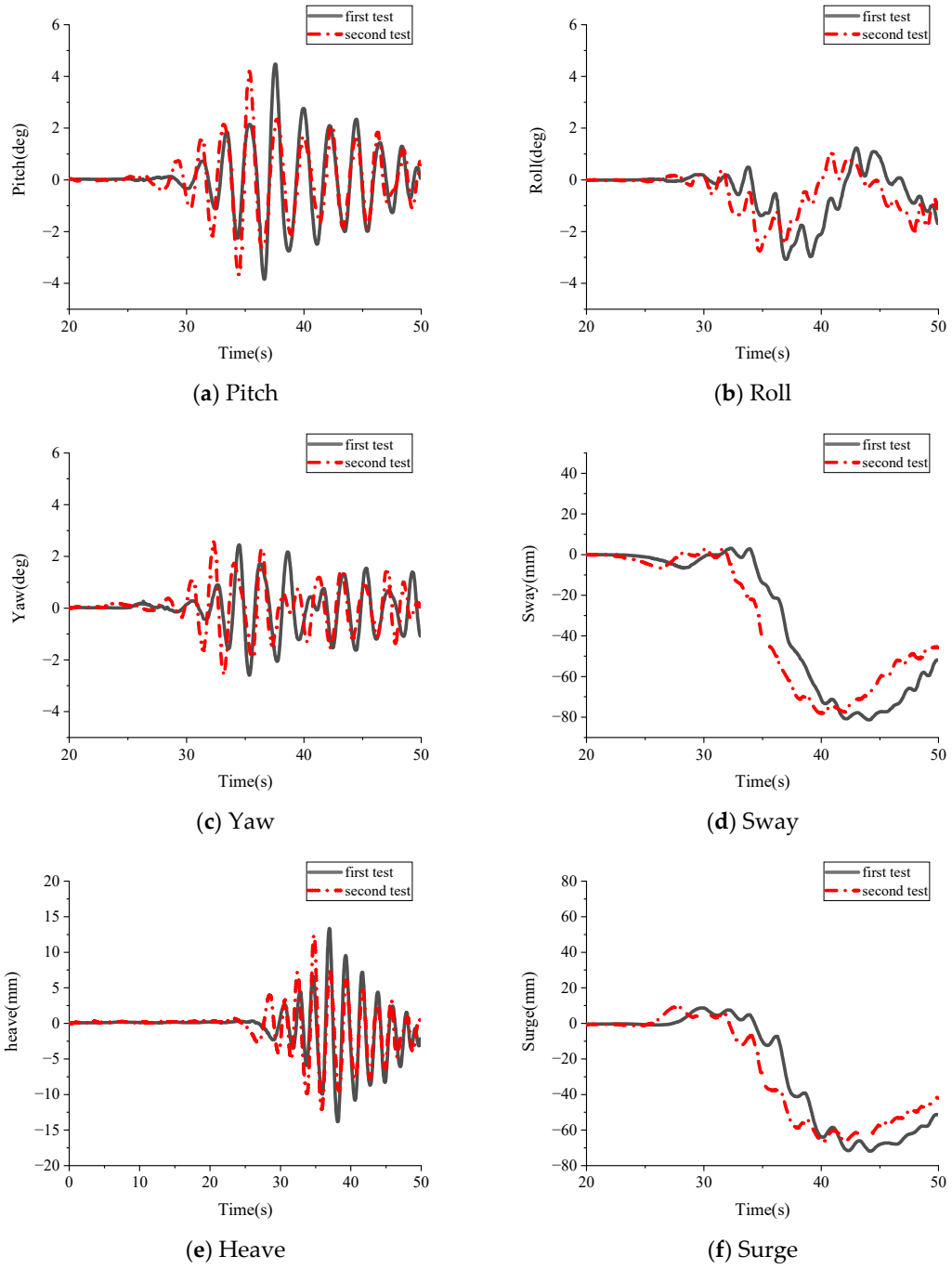

Figure 10. Two experimental tests under the same conditions (ship speed = 1.478 m/s, ship distance = 1.5 m, ship draft = 0.1 m).

4.1. The Influence of Regular Waves

Before conducting the subsequent control experiments, this research first carried out a systematic verification experiment on the motion response characteristics of the floating carrier of the mooring catamaran under the action of regular waves. The experiment adopted the control variable method and focused on investigating the influence of two key parameters, namely wave height (H = 0.02 m, 0.04 m, 0.06 m) and wave period (T = 1.2 s, 1.5 s), on the motion response of the carrier.

As shown in Figure 11, the experimental results show that the amplitude of the carrier's motion shows a significant increasing trend with the increase in wave height, and its variation law is in line with the prediction of the floating body response by the

linear wave theory. The motion response shows obvious periodic characteristics with the variation in the wave period, but the influence amplitude is relatively small, which is consistent with the frequency-domain response characteristics of the mooring float. The motion response curves collected in the steady-state stage have good repeatability and regularity. The consistency between the experimental data and the classical mooring float motion theory further verifies the scientific nature of the experimental method.

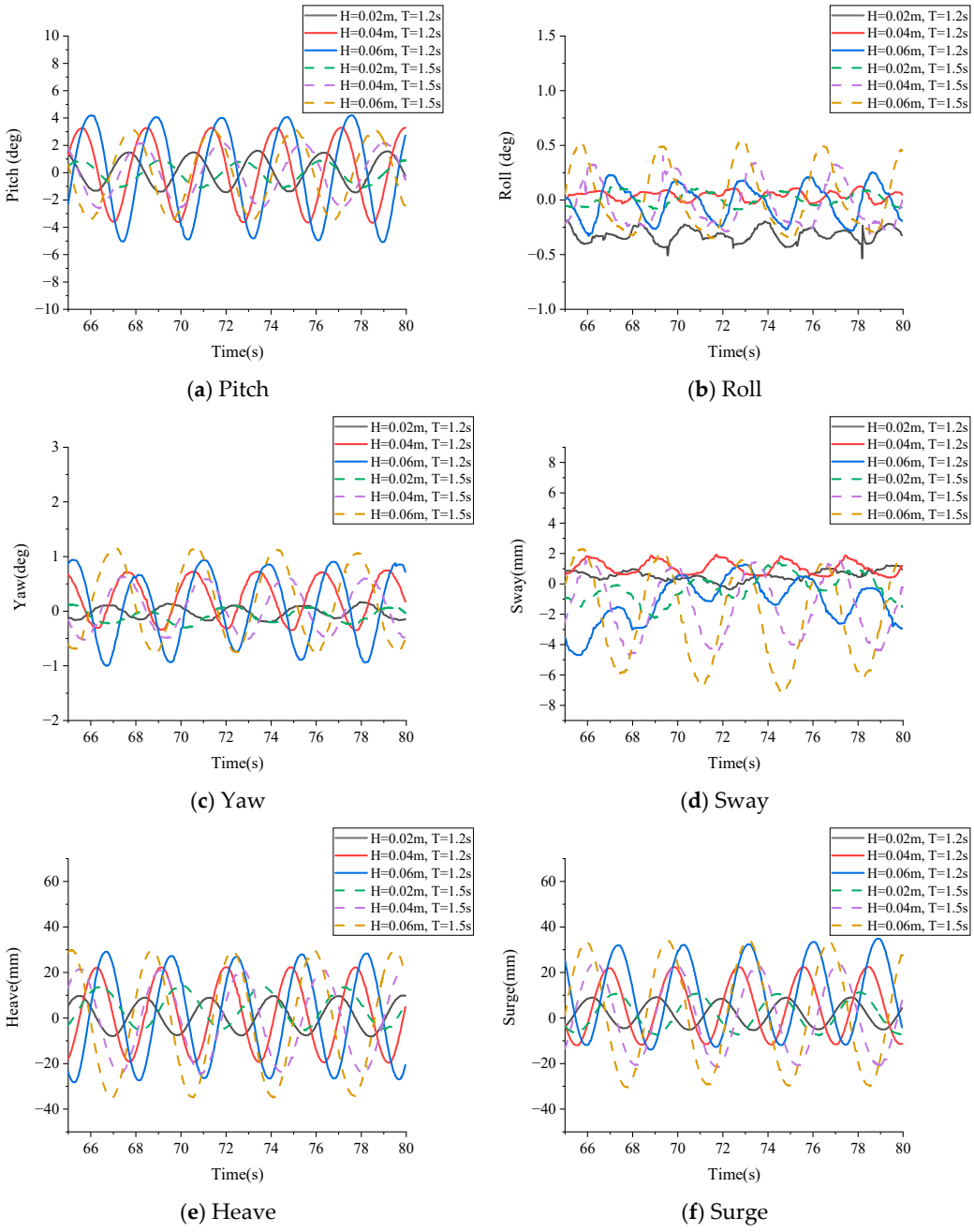

Figure 11. Carrier motion response under different regular wave conditions (no ship wave).

As shown in Figure 12, the change curves of the longitudinal and vertical oscillations of the regular wave with 0.02 m wave height and 1.5 s wave period were selected for comparison of the regular wave data, and the curves in the figure were extracted from the data after the motion of the carrier became relatively stable. It can be seen that the change rule of the curves is consistent, but due to the problem of simulation grid setting, there is regular wave attenuation, and the motion response appears to be reduced. At the

same time, in the experiment, due to the influence of external factors, the curve of the transverse rocking value change is not smooth, but the change interval is consistent with the simulation.

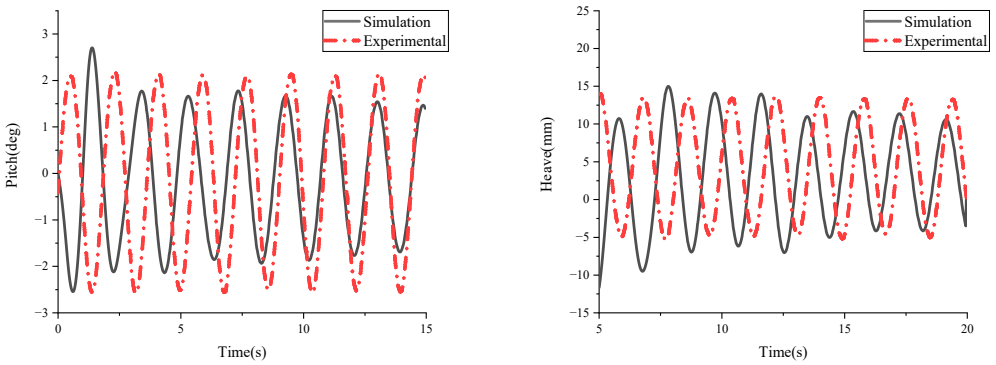

(**a**) Pitch (**b**) Heave

Figure 12. Comparison of experimental simulation data under same regular wave.

The peak values of longitudinal rocking and peak values of pendulum oscillations in the experiment and simulation under regular waves are shown in Table 6. By comparing the curve peaks, we found that the error of longitudinal rocking is about 5.9%, and the error value of drooping oscillation is about 9.6%, and the error values are all within 10%.

Table 6. Error between experimental and simulated amplitude of carrier motion response under regular wave.

Degrees of Freedom	Experimental Values	Simulated Values	Error
Pitch (°)	2.7	2.54	5.9%
Heave (°)	13.53	14.96	9.6%

4.2. The Influence of Ship Speeds

This research explored the effect of sailboat speed variation on the motion response of a moored catamaran through a controlled experiment. In the experiment, the distance between the sailboat and the catamaran was fixed at 1.5 m. The aim of the experiment was to investigate the effect of traveling waves on the six-degree-of-freedom motion of the catamaran at different boat speeds (0.3, 0.6, 0.9, 1.2, and 1.478 m/s). Given the limited width of the experimental tank, reflections from the tank wall observed during the experiment may have interfered with the results. To minimize the effect of this interference, experimental data collection was initiated when the sailboat started its motion and continued until the catamaran was most affected by the traveling wave, at which point data collection was stopped to ensure the accuracy of the data.

The time curve of the catamaran carrier model with the change in ship speed is shown in Figure 13. At low speed (0.3–0.9 m/s), the motion response of the catamaran carrier changes less; as the ship speed increases, the motion response changes show a dramatic change. When the ship speed exceeds 1.2 m/s, the motion response shows a significant jump. The peak of pitch ranges from 1.62° to 4.47°, the peak of roll ranges from 0.76° to 2.44°, the peak of yaw ranges from 0.23° to 1.22°, the peak of sway ranges from 35.37 mm to 81.74 mm, and the peak of heave ranges from 3.97 mm to 13.94 mm. By analyzing the variations, it can be seen that the magnitude of the influence of the ship's traveling wave on the motion response of each degree of freedom of the carrier is small in the low-speed range (0.3–0.9 m/s). This indicates that, at low speeds, the fluid perturbation energy is low, resulting in the relatively small kinematic response of the carrier. The kinetic energy of

the fluid at low speeds is not sufficient to cause significant fluctuations or disturbances, making the flow field around the carrier relatively smooth. The significant jump in the high-speed interval (1.2–1.478 m/s) reflects the nonlinear nature of the hydrodynamic forces. The complexity and dynamics of the hydrodynamic forces increase as the vessel speed increases, leading to a significant increase in the carrier motion response. This nonlinear effect is particularly evident at high speeds, suggesting that the influence of the ship wave on the stability of the carrier is more significant under high-speed conditions.

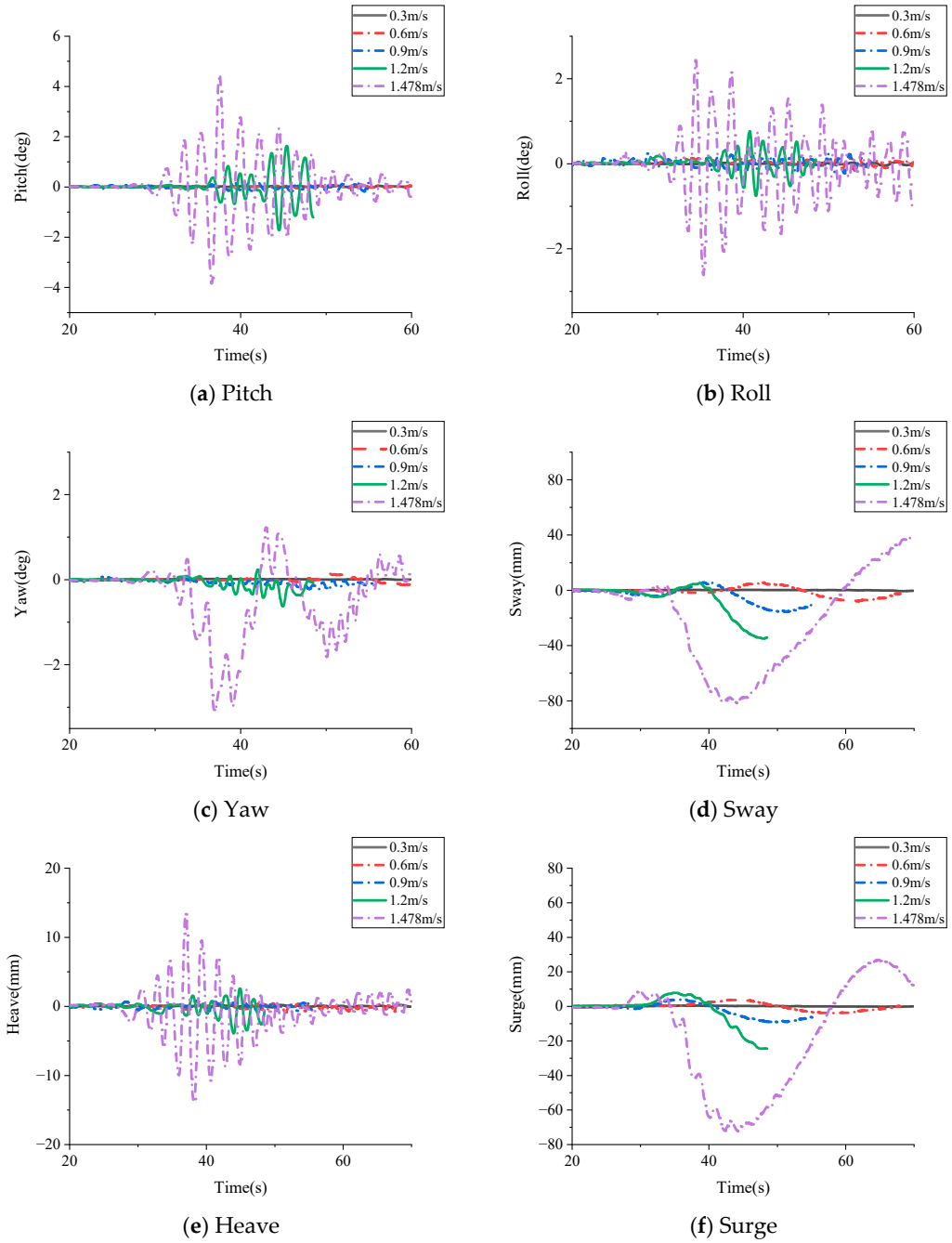

Figure 13. Carrier motion response at different ship speeds (ship distance = 1.5 m, ship draft = 0.1 m).

4.3. The Influence of the Distance Between Two Ships

Figure 14 reveals the significant effect of boat pitch on the six-degree-of-freedom kinematic response of the catamaran carrier. When the ship speeds are all 1.478 m/s, the roll remains stable (2.62° ± 0.03°), with the increase in ship distance being from 1.5 m to

2.5 m, indicating that it is less affected by the ship distance; the pitch decreases sharply by 40% (4.48°→2.69°), reflecting that the longitudinal perturbation of the ship's traveling wave attenuates rapidly with the distance; the yaw decreases by 64% (3.10°→1.13°), confirming the dominant effect of ship track flow on the steering moment of the carrier; surge decreases by 76% (72.3 mm→17.5 mm), and sway decreases by 55% (81.7 mm→36.8 mm), reflecting the exponential decay property of the wave force with the distance; and heave decreases by 27% (13.9 mm→10.2 mm), showing that the pendant movement has the lowest sensitivity to the distance of the ship.

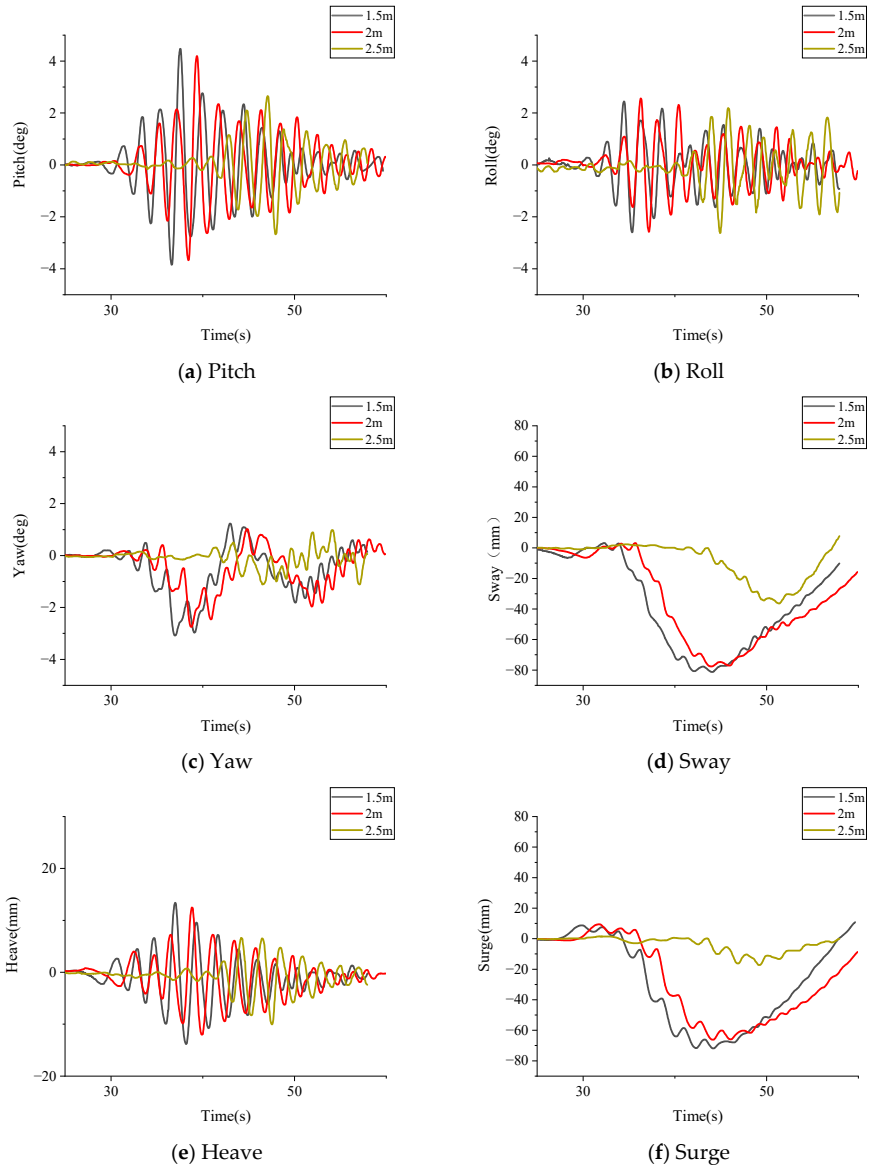

(**a**) Pitch (**b**) Roll

(**c**) Yaw (**d**) Sway

(**e**) Heave (**f**) Surge

Figure 14. Carrier motion response at ship speed of 1.5 m/s at different ship distances (no regular waves and ship draft = 0.1 m).

Overall, during the navigation of a ship, the distance between it and the carrier has a significant impact on the propagation of the ship's traveling waves and the motion response of the carrier. When the distance between the ship and the carrier gradually increases, the time for the ship's traveling wave to diffuse from the ship to the carrier will also be delayed accordingly. Meanwhile, the wave energy will gradually be consumed and attenuated during the long propagation path, which causes the wave energy received by the carrier to continuously weaken. Therefore, the motion response of the carrier will also decrease

accordingly, and the peak value of its motion response will gradually decrease with the increase in the ship distance. The influence of this distance on the propagation of ship traveling waves and the response of the carrier fully demonstrates the important role of the distance factor in the interaction between ships and carriers and also reveals the intrinsic connection between the propagation of ship traveling waves and the response of the carrier.

4.4. The Influence of Ship Draft

The experimental results in Figure 15 show that, under the conditions of a fixed ship distance (1.5 m) and ship speed (1.478 m/s), the change in ship load has a significant influence on the motion response of mooring catamarans. This research finds that, when the ship is in an empty load state (draft of 0.1 m), due to the shallower draft of the hull, the wave formation resistance increases, and the ship's traveling wave energy is concentrated and distributed in the horizontal plane, resulting in a significant increase in the horizontal plane motion responses, such as the pitch, yaw, sway, and surge of the floating body, compared with the full-load condition (draft of 0.2 m). When the ship is in the unloaded state (draft 0.1 m), due to the shallow draft of the hull, the formation of wave resistance increases; the ship's traveling wave energy is centrally distributed in the horizontal plane, resulting in pitch, yaw, sway, and surge waves that are larger; the transverse rocking moment mainly originates from the ship's transverse displacement, which is weakly correlated to the draught, meaning the increase or decrease in the draught has a small impact on it; and the value of the swaying motion is positively correlated to the draught, so the increase in the ship's draught is not significant. Therefore, the increase in the ship's draft will increase the influence on the carrier's heave motion.

4.5. The Superimposed Influence of Ship Waves and Regular Waves

Considering that the occurrence of ship traveling waves at sea is often accompanied by the influence of other waves, in the experiment, for this problem, conditions of superimposing ship traveling waves and regular waves were applied. As shown in Figure 16, the sailing direction of the KCS ship and the propagation direction of the rule wave are opposite to each other, and the ship-generated traveling wave and the rule wave act together on the catamaran model.

Here, the six-degree-of-freedom motion response of the catamaran floating body was compared under the conditions of a single 1.5 m/s ship speed regular wave, three different regular waves, and the superimposed wave generated by the superposition of the two.

According to the analysis results in Figure 17, it can be known that the influence of the regular wave on the motion response of the carrier manifests as periodic changes in all six degrees of freedom, but its fluctuation amplitude is relatively small. In contrast, under still-water conditions, the carrier is basically in a static state. However, as the sailing ships pass by, all six degrees of freedom of the carrier change significantly. Further analysis of the motion response curves after the superposition of regular waves and ship traveling waves revealed that, compared with the action of a single regular wave, the motion responses of the carrier in all six degrees of freedom under the superposition condition increased. Compared with the traveling wave effect of a single ship, under the superimposed condition, the longitudinal sway, lateral sway, bow sway, and lateral sway responses of the carrier are reduced, while the longitudinal sway and vertical sway responses are increased. This phenomenon can be attributed to the relative interaction between the direction of the traveling wave and the direction of the incoming regular wave: Since the ship begins to sail only after the regular wave reaches the carrier, the motion response of the carrier is first affected by the regular wave and then by the traveling wave.

The existence of regular waves has a certain inhibitory effect on the influence of ship waves, thereby leading to the variation characteristics of the above-mentioned motion response.

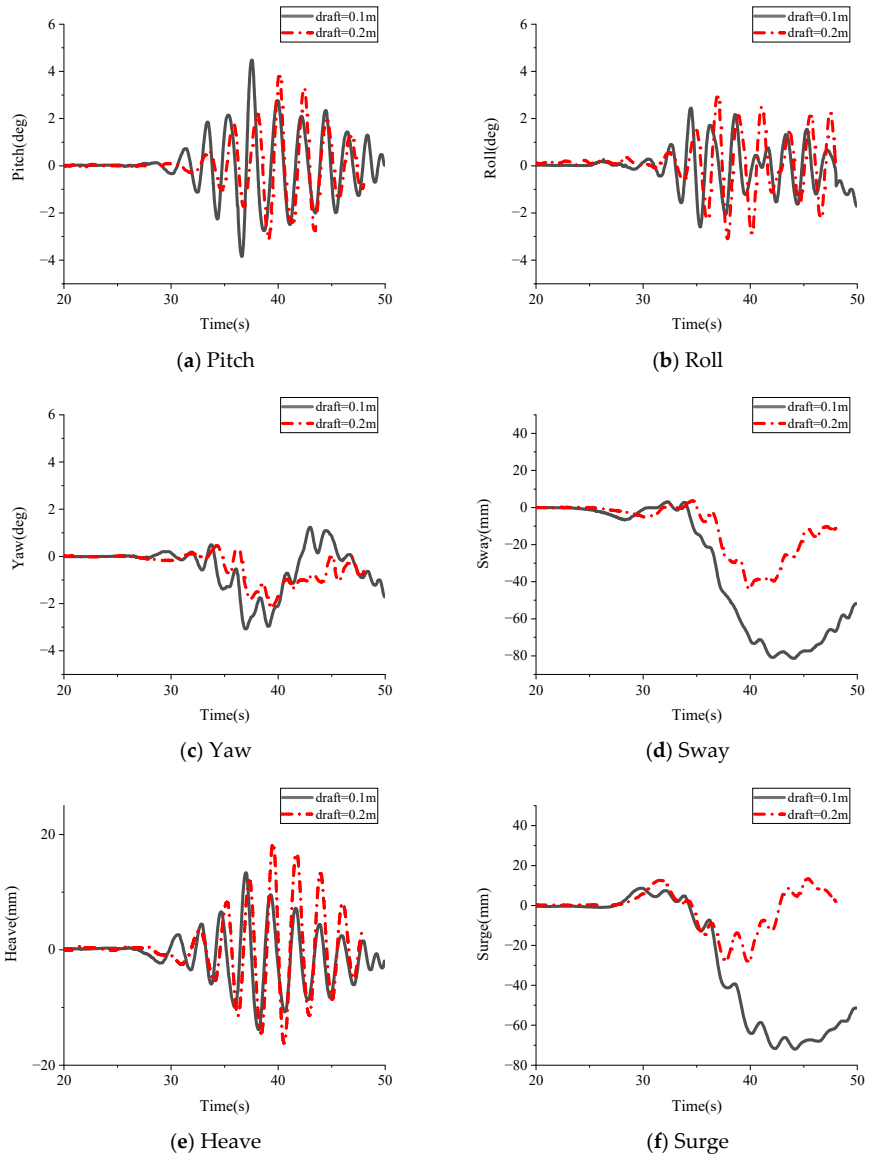

Figure 15. Carrier motion response at ship speed of 1.5 m/s at different ship draft values (no regular waves and ship distance = 1.5 m).

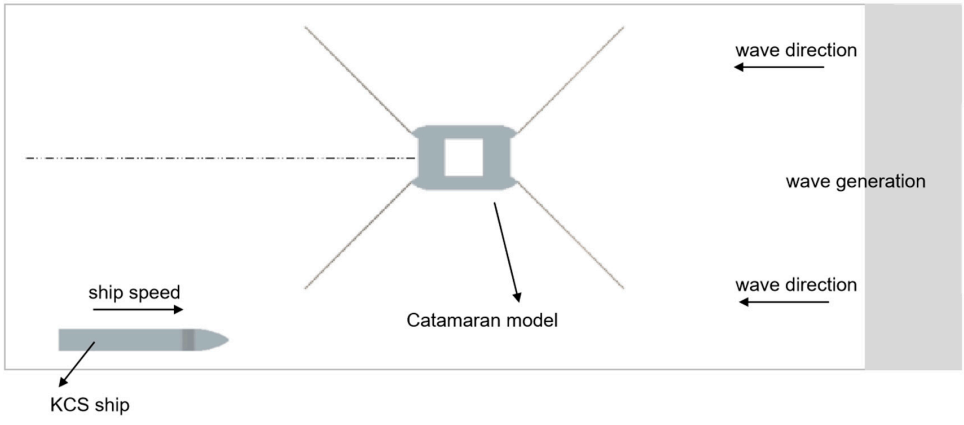

Figure 16. Ship navigation—regular wave direction.

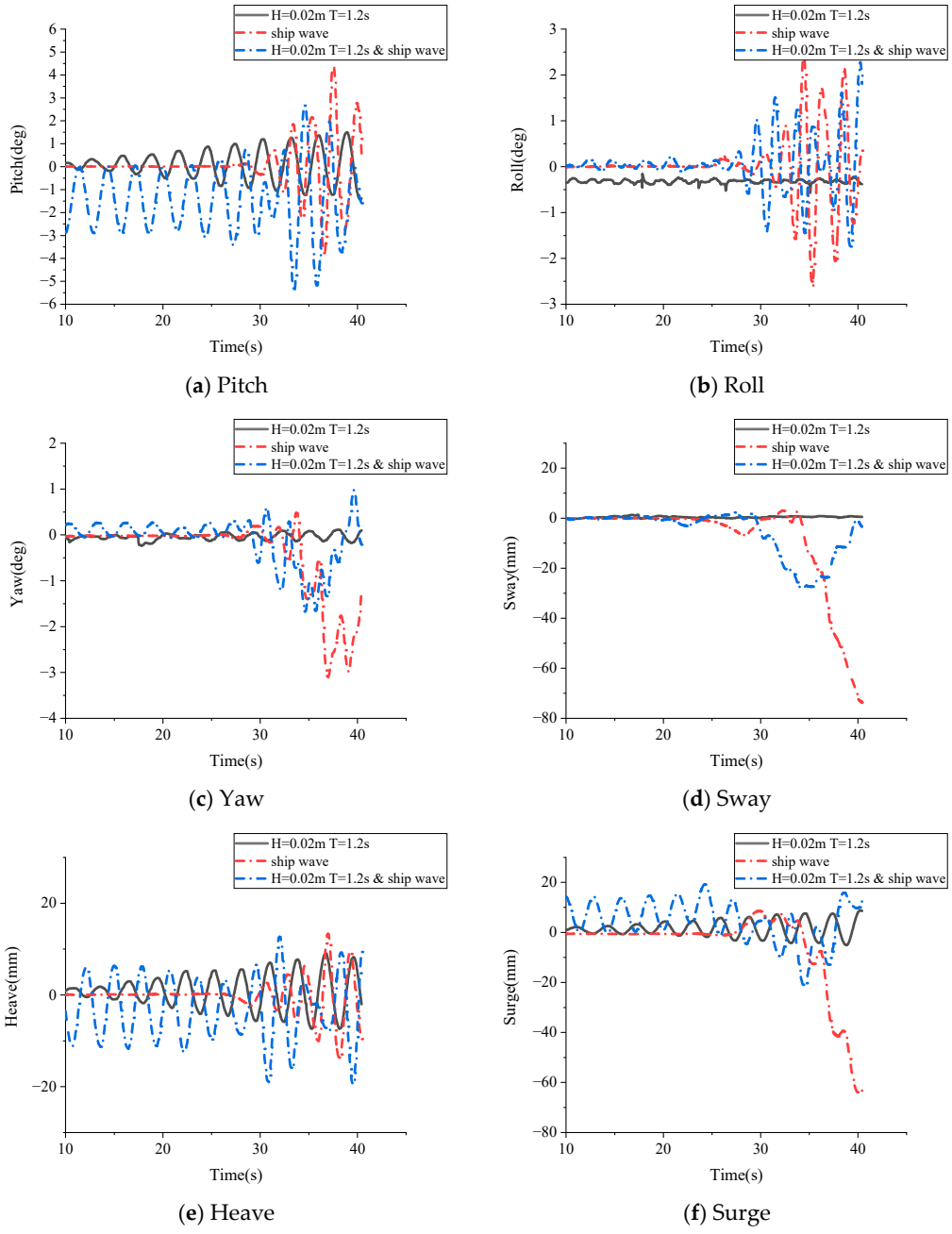

Figure 17. Comparison of the motion response curve caused by the superposition of 1.2–0.02 regular wave and ship movement wave (ship speed = 1.478 m/s, regular waves for wave height H = 0.02, and wave period T = 1.2 s, with cooperative interaction).

In order to verify whether the changes in the wave height and wave period of the regular wave have a certain inhibitory effect on the influence of the ship wave, the superposition conditions of 0.02 m wave height and 1.5 s wave period, as well as 0.04 m wave height and 1.2 s wave period with the ship wave, were applied. The variation curves of the six degrees of freedom over time are shown in Figure 18. It can be seen from the analysis of the curve that, under the condition of a single ship traveling wave, with the decrease in the period of the regular wave and the increase in the height of the regular wave, the changes in the six degrees of freedom all increase. Pitch, yaw, and heave are greatly affected by the changes in the regular wave. The change in roll is still dominated by the ship traveling wave, and the addition of the regular wave will only slightly reduce the amplitude of the change in roll. Due to the consideration of the influence of the tank wall effect, the data

collection for the longitudinal swing curve and the transverse swing is relatively short. However, it can be seen that, in terms of amplitude, the traveling wave still dominates.

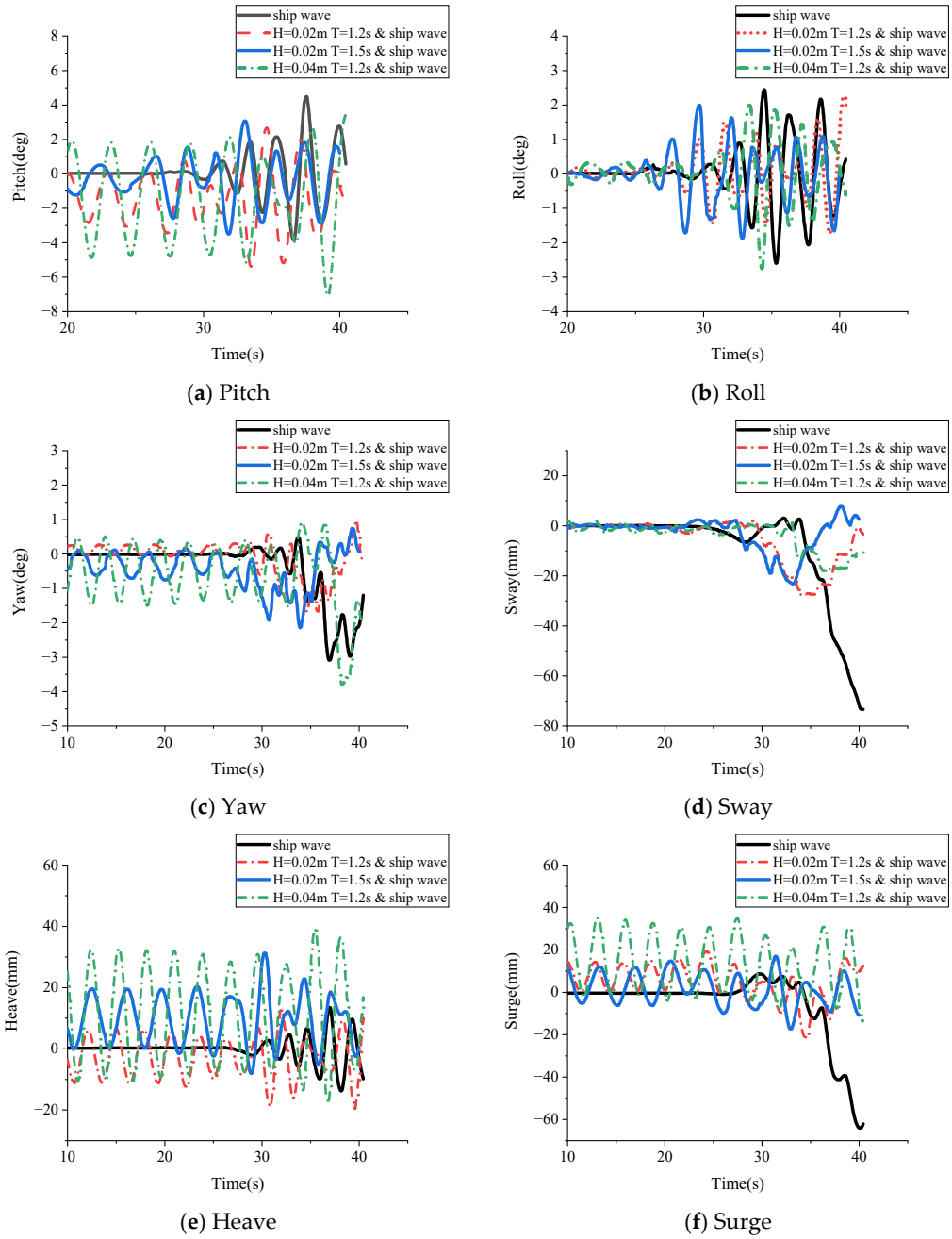

(**a**) Pitch (**b**) Roll

(**c**) Yaw (**d**) Sway

(**e**) Heave (**f**) Surge

Figure 18. Motion response curve of ship traveling wave superimposed by different regular waves (ship speed = 1.478 m/s, regular waves for wave height H = 0.02/0.04 m, and wave period T = 1.2 s/1.5 s).

5. Conclusions and Prospects

In this research, the motion response characteristics of a catamaran under the action of regular waves and ship traveling waves were investigated through physical model experiments, using a KCS ship as a sailing ship model and a catamaran as a carrier model of tidal current energy generating device, focusing on analyzing the influence of environmental parameters. The experiment used a scaled model to simulate different sea conditions in an experimental tank, and the six-degree-of-freedom motion response of the hull was

monitored in real time by a motion capture system. From the experimental results, we can draw the following conclusions:

(1) The influence of regular waves: As the wave height increases, the motion response of the carrier is significantly enhanced; the wave varies periodically, and the motion response shows periodic laws. The increase in the wave period has a certain influence on the motion response, but the influence is relatively small.

(2) The dominant influence of ship traveling waves: The parameters of ship traveling waves have a significant impact on the motion response of the carrier. As the speed of the ship increases, the amplitudes of each degree of freedom increase. When the ship distance increases, the influence of roll is small, the amplitudes of other degrees of freedom decrease, and the change is significant when the ship distance is 2.5 m. When the load of a ship increases, the amplitude of the motion response decreases, which is related to the ship type.

(3) Wave interaction under superimposed conditions: When regular waves and ship waves are superimposed, the amplitudes of roll and heave increase, while the amplitudes of sway and yaw decrease. The suppression efficiency is positively correlated with the steepness of the regular waves.

However, there are two limitations of this research:

1 Limitations of regular wave conditions: The current research only used regular waves as input conditions, which cannot accurately reflect the nonlinear characteristics of waves in the actual sea area. It is suggested that subsequent research introduces the random wave field described by the JONSWAP spectrum or Pierson–Moskowitz spectrum to improve the engineering simulation accuracy.

2 The singularity of ship traveling wave conditions: The current analysis is based on the ideal working condition of a single ship sailing in a straight line, which is insufficient in the research of the coupling mechanism between ship traveling waves and regular waves. For more expansive future research, we suggest using (1) multi-angle sailing conditions (oblique 30–60°) and (2) typical merchant ship types (e.g., 50,000-ton bulk carriers, 10,000-case container ships). A more generalized wave–float coupling dynamics model can be established through multi-parameter combination tests.

Author Contributions: Validation, T.L.; Data curation, Z.Y.; Writing—original draft, T.L.; Writing—review & editing, X.G.; Supervision, X.G. and Y.X.; Project administration, X.G. All authors have read and agreed to the published version of the manuscript.

Funding: This research was funded by the National Natural Science Foundation of China (Grant No.52271293) and Key R&D Plan Projects in Zhejiang Province (Grant No.2019C02087).

Data Availability Statement: The original contributions presented in this study are included in the article. Further inquiries can be directed to the corresponding author.

Conflicts of Interest: The authors declare no conflict of interest.

References

1. International Energy Agency. *World Energy Outlook 2020*; IEA Publications: Paris, France, 2020. [CrossRef]
2. European Commission. EU Strategy for Offshore Renewable Energy. EUR-Lex. COM/2020/741 Final, Brussels, Belgium. 19 November 2020. Available online: https://eur-lex.europa.eu/legal-content/EN/TXT/?uri=CELEX:52020DC0741 (accessed on 15 May 2025).
3. Roberts, O.; Williams, A.; Masters, I. Comparative analysis of power density in marine renewable energy sources. *Renew. Energy* **2021**, *172*, 1273–1286.
4. Dai, P.; Huang, Z.; Zhang, J. A modelling study of the tidal stream resource around Zhoushan Archipelago, China. *Renew. Energy* **2023**, *218*, 119234. [CrossRef]

5. Spicer, P.; Yang, Z.; Wang, T.; Deb, M. Spatially varying seasonal modulation to tidal stream energy potential due to mixed tidal regimes in the Aleutian Islands, AK. *Renew. Energy* **2025**, *253*, 123564. [CrossRef]
6. Sun, J.; Hu, J.L.S.; Li, H. A Laplace domain method for estimating wave elevation from the transient motion responses of floating structures. *J. Fluids Struct.* **2025**, *137*, 104338. [CrossRef]
7. Zang, Z.P.; Zong, H.M.; Fang, Z.; Zhang, J.; Hu, C. Experimental Study on the Motion Response Characteristics of a Floating Wind Turbine with a Semi-Submersible Foundation. *Water* **2025**, *17*, 1501. [CrossRef]
8. Wang, S.J.; Yu, X.L.; Li, R.J. Research on the Influence of Submerged Carriers on the Performance of Tidal Current Turbines. *J. Ocean. Technol.* **2016**, *35*, 1108–1112. (In Chinese)
9. Sheng, Q.H.; Li, C.; Zhang, X.W. Floating Vertical Axis Tidal Turbine Wave Load Analysis. *J. Ocean Technol.* **2016**, *35*, 25–28. (In Chinese)
10. Huang, Z.; Ouahsine, A.; Du, P.; Ding, D. Computational fluid dynamics predictions of critical hydrodynamics thresholds in the erodibility of inland waterway bank by ship-induced waves. *Ocean Eng.* **2022**, *266*, 112825. [CrossRef]
11. Zhang, Z.Q.; Zou, L.; Zou, Z.J. A Numerical Study on the Effects of Ship-Generated Waves on a Moored Ship in Restricted Waterways Considering Initial Acceleration Process. *J. Mar. Sci. Eng.* **2023**, *11*, 483. [CrossRef]
12. Wu, C.Q.; Li, M.H.; Luo, H.; Hu, T.; Yi, S.; Wang, G. Dynamic Response and Vibration Control of Deep-water Bridge Piers under Ship Wave Excitation. *Eng. Lett.* **2025**, *33*, 1871.
13. Zhang, H.J.; Liu, X.D.; Cao, X.Y.; Zhang, N.; Law, A.W.K. Dynamic response and power performance of a novel wind-wave-tidal energy system with single-point mooring integration. *Energy* **2025**, *325*, 136114. [CrossRef]
14. Ramli, L.N.; Mohamed, R.M.; Ibrahim, I.W.; Kurukuri, P. Enhanced Stability and Performance of the Tidal Energy Conversion System Using Adaptive Optimum Relation-Based MPPT Algorithms. *Arab. J. Sci. Eng.* **2025**. [CrossRef]
15. Rabaud, M.; Moisy, F. Prediction of ship-generated wave heights based on hull form parameters and speed. *Phys. Fluids* **2013**, *25*, 110804.
16. Kubo, M.; Saito, K.; Mizui, S.; Seto, J.; Seida, K. An Experrimental Study on Simulation of Irregular Waves Using Ship-Generated Waves. *J. Jpn. Inst. Navig.* **1996**, *95*, 351–359. [CrossRef]
17. Jonkman, J.; Matha, D. Frequency-domain analysis of floating structures under combined environmental loads. *J. Offshore Mech. Arct. Eng.* **2011**, *133*, 031103.
18. Ni, Y.P.; Li, Y.G. Current Situation and Development Trend of Active Absorption Wave-Making System for Wavemaker. *J. Mar. Eng.* **2019**, *12*, 123–135.
19. Van Oossanen, P.; Kim, J.H.; Hino, T.; Simonsen, B. A Comprehensive Experimental Database for the KRISO Container Ship (KCS). *J. Ship Res.* **2008**, *52*, 123–145.
20. Zhang, L.; Wang, Q.; Liu, Y. Hydrodynamic performance of a catamaran-type floating tidal energy platform. *Renew. Energy* **2022**, *189*, 1234–1245.
21. Ma, Y.; Hu, Z.; Xiao, L. Dynamic analysis of spread mooring systems for floating offshore wind turbines. *Ocean Eng.* **2023**, *280*, 114567.

Disclaimer/Publisher's Note: The statements, opinions and data contained in all publications are solely those of the individual author(s) and contributor(s) and not of MDPI and/or the editor(s). MDPI and/or the editor(s) disclaim responsibility for any injury to people or property resulting from any ideas, methods, instructions or products referred to in the content.